Carbon 138 (2018) 390–396

Contents lists available at ScienceDirect

Carbon

journal homepage: www.elsevier.com/locate/carbon

Enhanced exfoliation efficiency of graphite into few-layer graphene via reduction of graphite edge

Liangwei Yang [a], Fuzhen Zhao [a, b], Yan Zhao [a], Yangyong Sun [a], Guangwu Yang [b], Lianming Tong [a, *], Jin Zhang [a, **]

[a] Center for Nanochemistry, Beijing Science and Engineering Center for Nanocarbons, Beijing National Laboratory for Molecular Sciences, College of Chemistry and Molecular Engineering, Peking University, Beijing, 100871, China
[b] College of Science, China University of Petroleum, Qingdao, 266580, China

ARTICLE INFO

Article history:
Received 6 June 2018
Received in revised form
23 July 2018
Accepted 25 July 2018
Available online 25 July 2018

ABSTRACT

Graphene has received abundant attentions in many applications because of its extraordinary properties. Liquid-phase exfoliation is one of the most important methods to obtain graphene from graphite. However, due to strong van der Waals interaction force, it is still extremely challenging to further improve the exfoliation efficiency. Here we report that by carrying out reductions with the oxygenic functional groups on the pristine graphite edges using hydrazine hydrate and hydrogen at 800 °C as a pretreatment approach, the exfoliation efficiency can be improved by ~37% using a lithium-assisted liquid-phase exfoliation approach. The change of the functional groups is characterized by X-ray photoelectron spectroscopy and Fourier transform infrared spectroscopy. The graphene sheets show high degree of structural integrity and few defects. A thin film is prepared from the exfoliated graphene by vacuum assisted filtration and treated by annealing and mechanical compression. The graphene thin film shows a high thermal conductivity of 1707 $W m^{-1} K^{-1}$, which is superior to that of common metal materials, such as Cu and Al.

1. Introduction

Graphene is a single atomic-layer of hexagonal sp^2-bonded carbon atoms. Since its discovery, graphene has been attracting appreciable attention owing to its unique physical properties, including ultrahigh charge-carrier mobility (~10^6 $cm^2 V^{-1} s^{-1}$) [1], superior thermal conductivity (~5300 $W m^{-1} K^{-1}$) [2], optical transmittance (~97.7%) [3] and extremely intrinsic strength (~130 GPa) [4]. The mechanical exfoliation ("scotch-tape" method) of graphite into single and few-layer graphene nanosheets was discovered in 2004 [1–5]. Since then, many methods have also been developed to prepare large-scale or massive graphene. Chemical vapor deposition (CVD) was introduced to synthesize large-scale single-crystalline graphene films [6–8]. However, such CVD-grown graphene is usually costly and used in some particular applications such as optoelectronics and flexible electronics. Liquid-phase exfoliation of bulk graphite is acknowledged as the most widely used method for massive production of graphene [9–11]. Even though the quality of exfoliated graphene is relatively lower, the low-cost and mass production are extraordinarily advantageous for widespread applications in many fields such as polymer composites and clean energy devices.

Graphite is composited of graphene layers bonded together vertically through van der Waals force. In 2006, a solution-based method was reported to produce graphene oxide (GO) via chemical modification (strong oxidizing agents) of graphite, which has received great attention due to the capability of scalable production [12–14]. Reduced graphene oxide (rGO) can also be produced via the reduction of GO. GO can be well dispersed in the aqueous solution due to the existence of oxygenic functional groups, which, on the other hand, also destroy the structural integrity and bring many defects that cannot be completely repaired although after the reduction processes [15]. However, residual oxygenic functional groups of rGO are helpful in the application fields on the electrochemical catalysis [16] and composite with polymer [17]. Nevertheless, the oxide and reduce processes utilize abundant oxidizing and reducing agents, the post-treatment of which may bring up issues of high energy consumption and high pollution. Therefore, it

* Corresponding author.
** Corresponding author.
E-mail addresses: tonglm@pku.edu.cn (L. Tong), jinzhang@pku.edu.cn (J. Zhang).

https://doi.org/10.1016/j.carbon.2018.07.056
0008-6223/

is necessary to develop non-oxidizing method to produce graphene.

The Coleman group and others developed a simple non-oxide liquid-phase exfoliation of pristine graphite to produce high-quality graphene flakes using surfactants or organic solvents [9,18,19]. Although it is also considered as a promising method for mass production, the exfoliation efficiency is still too low to be industrialized. Alternatively, graphite can be intercalated to produce graphite intercalation compounds (GICs) by using various intercalates, such as alkali metals, organic molecules and transition metal halides [20]. GICs have been exfoliated to produce graphite nanoplatelets with thicknesses down to 2–10 nm [21–23]. According to the research of Jeon group, graphene flakes could be generated by using a eutectic system of ternary KCl–NaCl–$ZnCl_2$ salts through the intercalation process [24]. Li-GICs, formed by the insertion of lithium atoms in graphite, is a widely used anode material for Li-ion batteries (LIB). Because of the high activity of lithium, the exfoliation methods were inspired by the electrochemical reactions of negative electrodes in the rechargeable LIB [25,26]. Song et al. developed the lithium-assisted approach for the exfoliation of pristine graphite [27]. In this approach, Li/liquid ammonia solution was utilized to synthesize a lithium intercalated graphite precursor. Among all the methods that have been developed, the key challenge is still to increase the exfoliation efficiency of pristine graphite.

Graphite ore, the raw material of graphite powder, is mined by both open pit and underground processes (Figure S1). In these complicated processes, the regrinding and ball milling can decrease the size of raw materials at relatively high temperature, but may introduce numerous oxygenic functional groups on the graphite edges [28]. The regrinding and ball milling damage C-C bonds of graphite to form highly active carbon radical, which can be oxidized into oxygenic functional groups (carbonyl, epoxy and carboxyl) in the atmosphere. The heat produced by friction in the regrinding and ball milling provides enough energy for the functionalization reaction. As a result, the edges of the graphite used for LPE are defective and functionalized by oxygenic functional groups. To a certain extent, the stereo-hindrance effect of oxygenic functional groups will hinder the insertion of atoms and molecules. Hence, for more atoms to intercalate into the graphite interlayers for exfoliation, it is extremely needed to remove these oxygenic functional groups on the graphite edges.

Herein, we report a pre-reduction based approach to enhance the exfoliation efficiency of graphite into few-layer graphene via reduction of graphite edge. Before the exfoliation process, the oxygenic functional groups on the graphite edges were reduced by solution (hydrazine hydrate) and thermal (hydrogen, high temperature) approaches. After reduction, the stereo-hindrance effect of graphite edges was decreased and more Li atoms could intercalate into graphite interlayers in the lithium-assisted physical insertion. The change of the functional groups caused by the reduction reaction can be accurately characterized by X-ray photoelectron spectroscopy (XPS) and Fourier transform infrared spectroscopy (FT-IR). Due to the removal of oxygenic functional groups on the graphite edges, the exfoliation efficiency of lithium-assisted liquid-phase exfoliation was enhanced by ~37%. The average size of exfoliated graphene sheets was about 1 μm, and over 94% had no more than 5 layers. The electron diffraction patterns in Transmission Electron Microscope (TEM) shows that graphene sheets maintain high degree of structural integrity. A thin film of graphene was fabricated from the exfoliated graphene sheets using an annealing and mechanical compression process. The thermal conductivity of the film was found to be 1707 $W m^{-1} K^{-1}$, which is superior to common metal films (Cu and Al). This work demonstrates a feasible route to enhance the efficiency of LPE, and at the same time preserve the high quality of graphene.

2. Experimental

2.1. Materials and methods

Graphite powder (Figure S2) was bought from BTR new energy materials Inc. The following chemicals were used without further purification: lithium foil (AR, China Energy Lithium Co., LTD), hydrazine hydrate ($N_2H_4 \cdot H_2O$, 85%, Sinopharm Chemical Reagent Co., LTD), ethanol (C_2H_5OH, Bejing Tong Guang Fine Chemicals Company), liquid ammonia (NH_3, Beijing Nanfei Industry and Trade Co. LTD.), *N*-methyl pyrrolidone (NMP, Xilong Scientific Co., LTD), hydrochloric acid (HCl, ~37%, Xilong Scientific Co., LTD), AAO membrane (60 mm in diameter, 0.2 μm in pore size, Whatman).

The morphology and structure of graphene sheets and graphene films were characterized by Scanning Electron Microscopy (SEM, Hitachi S-4800) at an acceleration voltage of 1 kV and TEM (FEI Tecnai F30) at 300 kV. Raman spectroscopy (Horiba Jobin Yvon LabRAM HR 800, 514.5 nm) was used to characterize the defect and quality of exfoliated graphene sheets. XPS (Kratos Analytical Axis-Ultra spectrometer with Al Kα X-ray source) and FT-IR (Nicolet is50, ThermoFisher) were used to characterize the change of oxygenic functional groups on the pristine graphite and reduced graphite. Sheet resistance was measured by means of an Agilent 4155C semiconductor characterization system. Ultraviolet–vis spectroscopy (UV–vis, Perkin Elmer Lambda 950) was used to measure the transmittance of the graphene dispersion. Atomic force microscopy (AFM, Bruker Dimension Icon) was carried out to measure the thickness of graphene sheets and statistics the thickness distribution. At room temperature, the thermal conductivity was carried out by a self-heating method. The thermal image was investigated by thermal infrared imager (Optris PI 160).

2.2. Reduction of graphite powder with hydrazine hydrate and hydrogen

The powder of pristine graphite (1 g) with an average diameter of 200 μm was dispersed into deionized water (500 ml). Small amount of ethanol was also introduced to homogeneously disperse the graphite powder. The hydrazine hydrate (1 ml) was added and the resultant mixture was further stirred (~25 rpm) for 3 h at 90 °C. Then the graphite powder was filtrated and dried. The resultant graphite powder was put on a quartz boat and placed within a quartz tube inside the furnace. The tube was purged with argon (Ar, 300 sccm). Then the furnace was heated to 800 °C under Ar (300 sccm) and H_2 (100 sccm) flow at ambient pressure. The graphite powder were held at 800 °C for 1 h. The hydrazine hydrate and thermal annealing can ensure removing oxygenic functional groups as many as possible and residual materials (ethanol and hydrazine hydrate). Finally we can get the reduced graphite.

2.3. Preparation of graphene sheets and measurement of electrical conductivity

Reduced graphite was added to lithium in liquid ammonia, which was prepared by the cooling of ammonia at an acetone/dry ice bath. The mixture was stirred for 2 h, and then the ammonia was slowly evaporated by means of thermostatic bath after the acetone/dry ice bath was removed. Then hydrochloric acid (HCl, ~37%) was added into the residule with mild sonication. The black products was cleaned by deionized water and ethanol. Finally, the graphene sheets was dispersed into NMP. The graphene dispersion was centrifuged at 1000 rpm for 1 h and the supernatant dispersion was

carefully collected.

The graphene dispersions in NMP were dip-coated onto a fresh silicon wafer and then annealed in argon at 800 °C for 2 h. AFM was used to measure the height of graphene sheet, and a single-layer graphene sheet of 0.8 nm was chosen to characterize the electrical properity. Micro-gap Au (600 nm)/Cr (80 nm) electrodes with a gap of ~300 nm were fabricated onto the single-layer graphene sheet via electron beam lithography. Based on the resultant *I-V* profiles, the sheet resistance value Rs can be calculated by the equation $R_S = RW/L$, where R, W and L represent the resistance value, width and electrode gap length of the single-layer graphene sheet, respectively.

2.4. Preparation of graphene film

The graphene film was prepared by vacuum assisted filtration of well-dispersed graphene solution through AAO membrane. Then the graphene film was dried under vacuum at 80 °C for overnight before peeling off from the AAO membrane. The graphene film was annealed at 3000 °C for 3 h under Ar in a graphite furnace (Zhuzhou Hongya Electric-heating Equipment Co., LTD) and then compressed at 30 MPa for 1 h.

3. Results and discussion

3.1. Reduction of graphite powder and characterization

Hydrazine hydrate [29] and hydrogen [30], which are commonly used in the reduction reaction of GO, were used to reduce the oxygenic functional groups on the graphite edges. The low-resolution XPS spectrum (Fig. 1a) shows that the carbon-to-oxygen ratio (C/O ~30) of reduced graphite is much higher than that of pristine graphite (C/O ~15). The result indicates that the reduction approach is effective to remove oxygenic functional groups on the pristine graphite edges. The high-resolution XPS spectra (Fig. 1b) for the O1s region of the reduced graphite and the pristine graphite are distinctly different. The O1s spectrum of the reduced graphite consists of two major components arising from C=O (~532.6 eV) and C-O-C (~536.7 eV), and the O1s spectra of the pristine graphite is composed of two main components from C=O (~532.6eV) and O=C-O (~534.7eV). After reduction, the proportion of carboxyl decreases and the proportion of epoxy and carbonyl increases, which have smaller stereo-hindrance. Elemental analysis is also used to characterize the content of carbon, hydrogen and nitrogen in the graphite powder (Figure S3). However, the graphite powder can not be completely decomposed because of trace impurities. After reduction reaction, the content of carbon and hydrogen increase. FT-IR characterization shows the direct evidence of the appearance of C—H bonds. The absorption bands near 2800 cm^{-1} of the reduced graphite can be assigned to C—H stretching modes (Fig. 1c), which is absent in the pristine graphite [31,32]. These results indicate that, those oxygenic functional groups of pristine graphite were not completely reduced in the reduction approaches. The diameter of carbonyl, epoxy and carboxyl is about 0.12 nm, 0.21 nm and 0.29 nm. And the diameter of lithium atom is about 0.32 nm [33]. The interlayer spacing of graphite is 0.334 nm, which is comparable to the size of the oxygenic functional groups. Due to the much lower oxygen content and smaller stereo-hindrance of oxygenic functional groups in the reduced graphite edges, more Li atoms can intercalate into the interlayer of graphite from the edges. The decrease of oxygen content and the change of functional groups are beneficial to the intercalation of more Li atoms.

3.2. Exfoliation preparation and characterization of graphene nanosheets

The lithium intercalation and the exfoliation for few-layer graphene are illustrated in Fig. 2a. As shown in Figure S2, the average size and thickness of the reduced graphite are respectively about 200 and 20 μm. As lithium can be easily dissolved in anhydrous ammonia, Lithium/liquid ammonia was used to produce Li-GIC [34]. The graphene sheets are exfoliated along with the release of H_2, which is the product of Li-GIC and HCl solution [27]. The as-prepared graphene sheets were then dispersed in *N*-methyl pyrrolidone (NMP) by sonication at a concentration of 0.5 mg ml^{-1}. The good dispersion was evidenced by the observation of Tyndall effect (Figure S4). The structural integrity and defect degree of graphene sheets were characterized by TEM. A droplet of diluted graphene suspension was dropped onto Cu grid and then annealed at the presence of argon at 500 °C for 2 h. Fig. 2b shows the bright-field TEM images of graphene samples. The central part of graphene

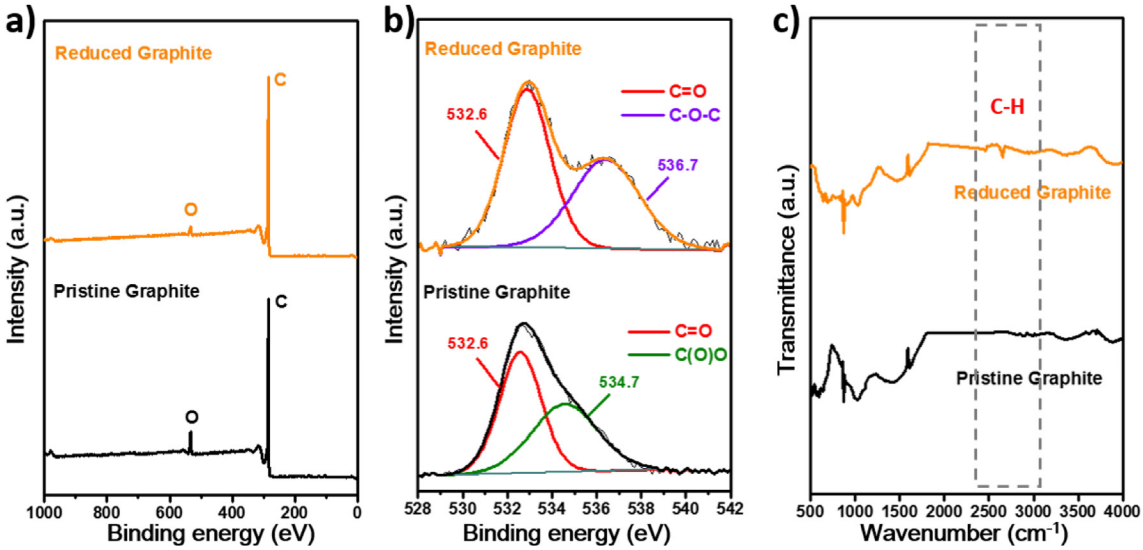

Fig. 1. The oxygenic functional groups on the graphite edges are reduced by solution approach and thermal approach. a, b) XPS survey a) and high-resolution O1s b) spectra of pristine graphite and reduced graphite. c) FT-IR of pristine graphite and reduced graphite. (A colour version of this figure can be viewed online.)

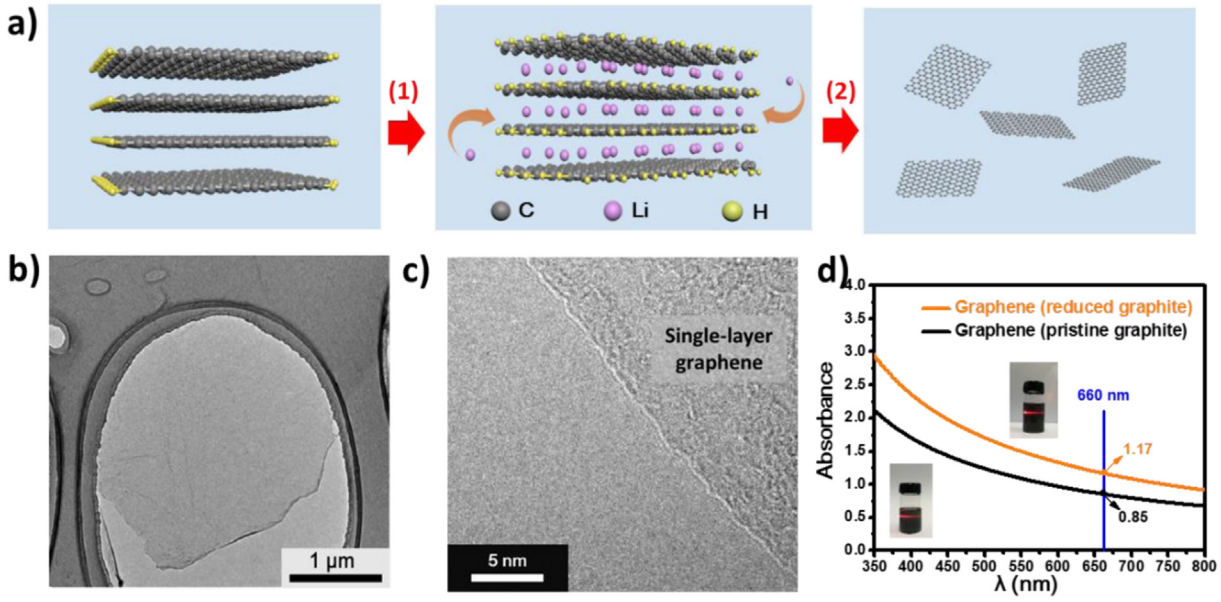

Fig. 2. Exfoliation of reduced graphite into few-layer graphene via lithium intercalation. a) Schematic illustration of Lithium atoms intercalation (1) and exfoliation (2). b) Typical TEM micrograph and c) HR-TEM micrograph at the edge of graphene sheet. d) The contrast of concentrations of graphene dispersions produced from pristine graphite and reduced graphite via UV–vis spectroscopy. (inset: graphene dispersions in NMP). (A colour version of this figure can be viewed online.)

sheet in the TEM image is uniform and indistinctive, and the edges partially scroll. In the TEM image, each layer typically shows a dark line on graphene edges [35]. There is no noticeable dark lines at the graphene sheet edge in high-resolution TEM (HR-TEM) image (Fig. 2c). The selected-area electron diffraction (SAED) patterns in Figure S4 shows that the intensity curve of line section through the (1−210)–(0−110)–(−1010)–(−2110) axis. The peak intensity of (1−210) and (−2110) is less than that of (0−110) and (−1010) in our experiments, confirming that the graphene nanosheet is single layer [9].

In order to compare the exfoliation efficiency, we exfoliated the same quality of pristine graphite and reduced graphite using the same method. After intercalation, exfoliation processes, and centrifugation at 1000 rpm for 60 min (see experimental section for details), the supernatant dispersion was kept. The two samples of as-prepared graphene powder were respectively dispersed into the same volume of NMP. UV–vis–IR absorption spectroscopy is used to characterize the concentration of these two dispersions. Because of the same solvent (NMP) and similar composition (Fig. 3c and Figure S5 and S6), the two dispersions have the same absorbance coefficient in the Lambert-Beer Law [9]. So the concentration is proportional to its absorbance. The optical absorbance (@660 nm) [9] of graphene dispersion from reduced graphite (1.17) outperformed the graphene dispersion from pristine graphite (0.85) by ~37% (Fig. 2d). The result shows that the exfoliation efficiency of graphite into few-layer graphene was enhanced via the reduction of graphite edges. Fig. 3a shows the Raman spectra of graphene sheet. This resultant spectrum contains three features: the D-peak at 1350 cm^{-1}, the G-peak at 1580 cm^{-1} and the 2D-peak at 2700 cm^{-1}. The D-peak, corresponding to first order of zone-boundary phonons, is present as the defects or edges effect of graphene [36]. So the degree of defects can be simply estimated by the relative intensity of D-peak and G-peak (I_D/I_G). The exfoliated graphene showed an I_D/I_G ratio of 0.2, relatively higher than that of pristine graphite (~0.06), mainly resulted from the small domain and ineluctable edge defects of graphene sheets.

The thicknesses of the graphene nanosheets were measured by AFM. The graphene dispersions in NMP were dip-coated onto a fresh silicon wafer and then annealed in argon at 800 °C for 2 h. The AFM image in Fig. 3b shows the heights of 0.79, 0.80 and 0.85 nm. The height of single layer graphene sheet is usually less 0.8 nm [37]. From the statistical analysis of 107 graphene nanosheets (average size: ~1.14 μm, Figure S5), most of these isolated graphene nanosheets (~94%) have the thickness of 0.6–2.0 nm (≤5 layers) while ~23% of these graphene nanosheets have single layer. The thickness histogram indicates the high selectivity of the exfoliation method. Furthermore, the sheet resistance of the single-layer graphene sheet is $1.12 \pm 0.15\ k\Omega \cdot sq^{-1}$ (Fig. 3d and Figure S7).

3.3. Preparation of high conductive graphene film

A thin film of graphene was prepared by vacuum assisted filtration of the well-dispersed graphene solution through Anodic Aluminum Oxide (AAO) membrane. Then the graphene film was dried under vacuum at 80 °C for overnight before being peeled off from the AAO membrane. The graphene film, produced via reduction of GO film, shows relatively high thermal conductivity [38]. A GO film needs as long as several days to be prepared [11]. The period of the preparation of graphene film is much shorter than that of GO film obtained through vacuum assisted filtration. This could be attributed to the less compact stack in the as-prepared graphene film (Fig. 4a). The thermal conductivity of the as-prepared graphene film was as low as 186 W/m K. This is due to the existence of gaps between layers of graphene, which are usually filled with air of thermal conductivity 0.024 $W\ m^{-1}\ K^{-1}$. To increase the thermal conductivity of the graphene film, thermal annealing and mechanical compression were applied [39]. The graphene film was annealed at 3000 °C for 3 h and then compressed mechanically under 30 MPa for 1 h. After the annealing and mechanical compression, the surface of graphene film became much smoother, and the gaps between graphene nanosheets disappeared. The thickness of the film decreased from 72 to 23.3 μm (Fig. 4b). XPS characterization shows that negligible oxygen was introduced after high temperature and compression procedure (C/O ~100, Figure S8). The high-resolution XPS spectrum for the C1s region (Figure S8) shows that treated graphene film had extremely high

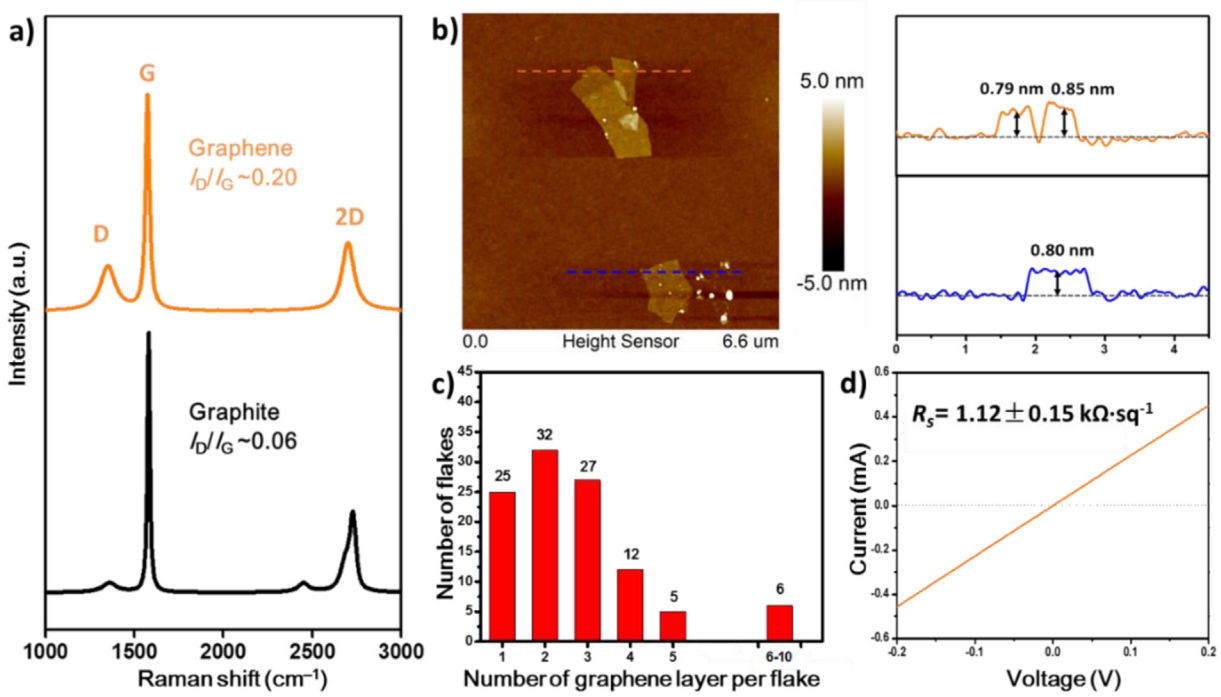

Fig. 3. Microscopic characterization and structural integrity of graphene sheets. a) Raman spectra of graphene sheets and pristine graphite. b) AFM image of there graphene sheets with their thickness profiles. c) Thickness histograms (AFM) of 107 selected graphene sheets. d) Electrical conductivity of the graphene sheets. (A colour version of this figure can be viewed online.)

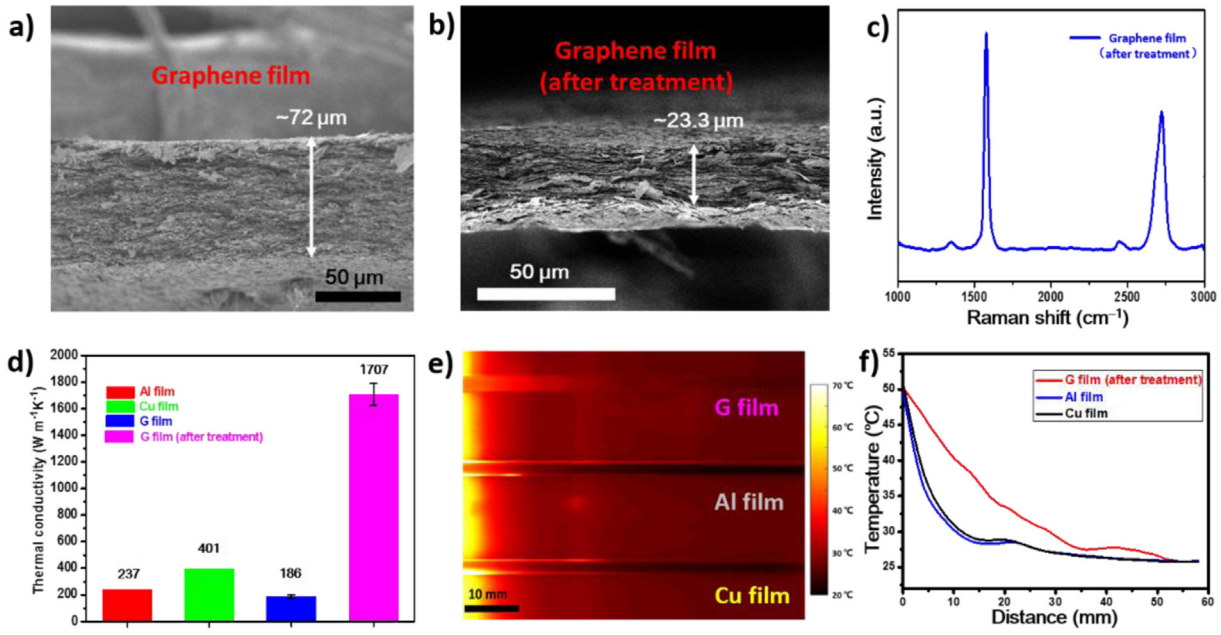

Fig. 4. Thermal conductivity of graphene film. a, b) SEM images of cross-sectional morphologies of graphene film before and after treatment. c) Raman spectra of graphene film after treatment. d) Comparison of thermal conductivities of Cu, Al, and graphene film before and after treatment. e) Comparison of infrared thermal images of Cu, Al and treated graphene film. All of material films have a thickness of ~20 μm. f) The temperature profiles of these three samples. (A colour version of this figure can be viewed online.)

purity in the graphitized sp^2-bonded carbon structure. Meanwhile, the intensity ratio of D-peak and G-peak (Fig. 4c) in Raman spectra decreased to as low as 0.01. These results indicate that carbon atoms in graphene sheets are highly compressed. As a result, the thermal conductivity of treated graphene film increased to 1707 $W\,m^{-1}\,K^{-1}$ (Fig. 4d). Infrared imaging was employed to visually compare the heat conduction rate of three films of different materials, that is, graphene, Al and Cu. The result clearly shows that the heat-transfer in the treated graphene film is more rapid than Al and Cu, which are commonly used for heat dispersion in electronic devices. The thermal conductivity of copper and aluminum are respectively 401 and 237 $W\,m^{-1}\,K^{-1}$ (Fig. 4e and f) [40,41]. The

ultrahigh thermal conductivity of treated graphene film is due to two main factors: good contact between graphene sheets and high graphitized crystallization. The thermal conductivity of graphene is contributed by phonon and electron transport [2]. However, based on the Kiedemann-Franz law, the contribution of electron transport in graphene can be ignored at room temperature [2]. The high crystallization via thermal annealing and improved contact between graphene sheets via mechanical compression are beneficial for the less phonon scattering in the graphene film.

4. Conclusion

In conclusion, we have demonstrated the enhancement of exfoliation efficiency of graphite into few-layer graphene via reduction of graphite edges. The regrinding and ball milling processes on the mined graphite ore cause numerus oxygenic functional groups (carbonyl, epoxy and carboxyl) on the graphite edges. These oxygenic functional groups hinder Li atoms to intercalate into the graphite interlayers. We utilize hydrazine hydrate and hydrogen to reduce the oxygenic functional groups before lithium-assisted LPE approach. Compared with pristine graphite, the exfoliation efficiency of reduced graphite into few-layer graphene nanosheets is enhanced by ~37%. The graphene nanosheets show negligible defects and maintain high degree of structural integrity. After annealing and mechanical compression, the thermal conductivity of graphene film is as high as 1707 W m^{-1} K^{-1}. We believe that the reduction of the graphite edges offers a feasible route to enhance the exfoliation efficiency of pristine graphite into few-layer graphene nanosheets. This method may be useful for large-scale production of graphene with improved quality.

Acknowledgements

The authors thank Prof. Changhong Liu and Zheng Duan (Tsinghua-Foxconn Nanotechnology Research Center and Department of Physics, Tsinghua University, Beijing) for help on measuring thermal conductivity of graphene film. The authors thank Chen Yin from Peking University for data collection of low-magnification and aberration-corrected atomic-resolved TEM image of graphene. This work was supported by the Ministry of Science and Technology of China (2016YFA0200101 and 2016YFA0200104), the National Natural Science Foundation of China (Grant Nos. 51432002, 51720105003 and 21790052), and the Beijing Municipal Science and Technology Project (Grant No. Z161100002116026).

Appendix A. Supplementary data

Supplementary data related to this article can be found at https://doi.org/10.1016/j.carbon.2018.07.056.

References

[1] K.S. Novoselov, A.K. Geim, S.V. Morozov, D. Jiang, Y. Zhang, S.V. Dubonos, et al., Electric field effect in atomically thin carbon films, Science 306 (5696) (2004) 666–669.
[2] A.A. Balandin, Thermal properties of graphene and nanostructured carbon materials, Nat. Mater. 10 (8) (2011) 569–581.
[3] R.R. Nair, P. Blake, A.N. Grigorenko, K.S. Novoselov, T.J. Booth, T. Stauber, et al., Fine structure constant defines visual transparency of graphene, Science 320 (5881) (2008) 1308.
[4] C. Lee, X. Wei, J.W. Kysar, J. Hone, Measurement of the elastic properties and intrinsic strength of monolayer graphene, Science 321 (5887) (2008) 385–388.
[5] A.K. Geim, K.S. Novoselov, The rise of graphene, Nat. Mater. 6 (3) (2007) 183–191.
[6] P.R. Somani, S.P. Somani, M. Umeno, Planer nano-graphenes from camphor by CVD, Chem. Phys. Lett. 430 (1–3) (2006) 56–59.
[7] Y. Hao, M.S. Bharathi, L. Wang, Y. Liu, H. Chen, S. Nie, et al., The role of surface oxygen in the growth of large single-crystal graphene on copper, Science 342 (6159) (2013) 720–723.
[8] T. Wu, X. Zhang, Q. Yuan, J. Xue, G. Lu, Z. Liu, et al., Fast growth of inch-sized single-crystalline graphene from a controlled single nucleus on Cu-Ni alloys, Nat. Mater. 15 (1) (2016) 43–47.
[9] Y. Hernandez, V. Nicolosi, M. Lotya, F.M. Blighe, Z. Sun, S. De, et al., High-yield production of graphene by liquid-phase exfoliation of graphite, Nat. Nanotechnol. 3 (9) (2008) 563–568.
[10] K.R. Paton, E. Varrla, C. Backes, R.J. Smith, U. Khan, A. O'Neill, et al., Scalable production of large quantities of defect-free few-layer graphene by shear exfoliation in liquids, Nat. Mater. 13 (6) (2014) 624–630.
[11] D.A. Dikin, S. Stankovich, E.J. Zimney, R.D. Piner, G.H. Dommett, G. Evmenenko, et al., Preparation and characterization of graphene oxide paper, Nature 448 (7152) (2007) 457–460.
[12] S. Stankovich, R.D. Piner, S.T. Nguyen, R.S. Ruoff, Synthesis and exfoliation of isocyanate-treated graphene oxide nanoplatelets, Carbon 44 (15) (2006) 3342–3347.
[13] W.C. Ren, H.M. Cheng, The global growth of graphene, Nat. Nanotechnol. 9 (10) (2014) 726–730.
[14] Y. Lu, G. Long, L. Zhang, T. Zhang, M. Zhang, F. Zhang, et al., What are the practical limits for the specific surface area and capacitance of bulk sp^2 carbon materials? Sci. China Chem. 59 (2) (2016) 225–230.
[15] Y.W. Zhu, S. Murali, W.W. Cai, X.S. Li, J.W. Suk, J.R. Potts, et al., Graphene and graphene oxide: synthesis, properties, and applications, Adv. Mater. 22 (35) (2010) 3906–3924.
[16] Y. Liang, Y. Li, H. Wang, J. Zhou, J. Wang, T. Regier, et al., Co_3O_4 nanocrystals on graphene as a synergistic catalyst for oxygen reduction reaction, Nat. Mater. 10 (10) (2011) 780–786.
[17] H. Kim, A.A. Abdala, C.W. Macosko, Graphene/polymer nanocomposites, Macromolecules 43 (16) (2010) 6515–6530.
[18] M. Lotya, Y. Hernandez, P.J. King, R.J. Smith, V. Nicolosi, L.S. Karlsson, et al., Liquid phase production of graphene by exfoliation of graphite in surfactant/water solutions, J. Am. Chem. Soc. 131 (10) (2009) 3611–3620.
[19] U. Khan, A. O'Neill, M. Lotya, S. De, J.N. Coleman, High-concentration solvent exfoliation of graphene, Small 6 (7) (2010) 864–871.
[20] M.B. Dines, Intercalation in layered compounds, J. Chem. Educ. 51 (4) (1974) 221–223.
[21] A. Charlier, M.F. Charlier, D. Fristot, Binary graphite-intercalation compounds, J. Phys. Chem. Solid. 50 (10) (1989) 987–996.
[22] A. Gruneis, C. Attaccalite, A. Rubio, D.V. Vyalikh, S.L. Molodtsov, J. Fink, et al., Angle-resolved photoemission study of the graphite intercalation compound KC_8: a key to graphene, Phys. Rev. B 80 (7) (2009) 075431.
[23] L.M. Viculis, J.J. Mack, O.M. Mayer, H.T. Hahn, R.B. Kaner, Intercalation and exfoliation routes to graphite nanoplatelets, J. Mater. Chem. 15 (9) (2005) 974–978.
[24] K.H. Park, B.H. Kim, S.H. Song, J. Kwon, B.S. Kong, K. Kang, et al., Exfoliation of non-oxidized graphene flakes for scalable conductive film, Nano Lett. 12 (6) (2012) 2871–2876.
[25] J.Z. Wang, K.K. Manga, Q.L. Bao, K.P. Loh, High-Yield synthesis of few-layer graphene flakes through electrochemical expansion of graphite in propylene carbonate electrolyte, J. Am. Chem. Soc. 133 (23) (2011) 8888–8891.
[26] Y.L. Zhong, T.M. Swager, Enhanced electrochemical expansion of graphite for in situ electrochemical functionalization, J. Am. Chem. Soc. 134 (43) (2012) 17896–17899.
[27] M.W. Xu, H.T. Sun, C. Shen, S. Yang, W.X. Que, Y. Zhang, et al., Lithium-assisted exfoliation of pristine graphite for few-layer graphene nanosheets, Nano Res 8 (3) (2015) 801–807.
[28] I.Y. Jeon, H.J. Choi, S.M. Jung, J.M. Seo, M.J. Kim, L.M. Dai, et al., Large-scale production of edge-selectively functionalized graphene nanoplatelets via ball milling and their use as metal-free electrocatalysts for oxygen reduction reaction, J. Am. Chem. Soc. 135 (4) (2013) 1386–1393.
[29] S. Park, R.S. Ruoff, Chemical methods for the production of graphenes, Nat. Nanotechnol. 4 (4) (2009) 217–224.
[30] Z.S. Wu, W.C. Ren, L.B. Gao, B.L. Liu, C.B. Jiang, H.M. Cheng, Synthesis of high-quality graphene with a pre-determined number of layers, Carbon 47 (2) (2009) 493–499.
[31] J.O. Sofo, A.S. Chaudhari, G.D. Barber, Graphane: a two-dimensional hydrocarbon, Phys. Rev. B 75 (15) (2007) 153401.
[32] H. Peelaers, A.D. Hernandez-Nieves, O. Leenaerts, B. Partoens, F.M. Peeters, Vibrational properties of graphene fluoride and graphane, Appl. Phys. Lett. 98 (5) (2011) 051914.
[33] J.C. Slater, Atomic radii in crystals, J. Chem. Phys. 41 (10) (1964) 3199–3204.
[34] Y. Vasil'ev, D. Wallis, M. Nuchter, B. Ondruschka, A. Lobach, T. Drewello, From major to minor and back - a decisive assessment of $C_{60}H_{36}$ with respect to the Birch reduction of C-60, Chem. Commun. (J. Chem. Soc. Sect. D) 14 (2000) 1233–1234.
[35] X. Jia, J. Campos-Delgado, M. Terrones, V. Meunier, M.S. Dresselhaus, Graphene edges: a review of their fabrication and characterization, Nanoscale 3 (1) (2011) 86–95.
[36] A.C. Ferrari, J.C. Meyer, V. Scardaci, C. Casiraghi, M. Lazzeri, F. Mauri, et al., Raman spectrum of graphene and graphene layers, Phys. Rev. Lett. 97 (18) (2006) 187401.
[37] K. Parvez, Z.S. Wu, R.J. Li, X.J. Liu, R. Graf, X.L. Feng, et al., Exfoliation of graphite into graphene in aqueous solutions of inorganic salts, J. Am. Chem. Soc. 136 (16) (2014) 6083–6091.
[38] S.Y. Huang, B. Zhao, K. Zhang, M.M. Yuen, J.B. Xu, X.Z. Fu, et al., Enhanced

reduction of graphene oxide on recyclable Cu foils to fabricate graphene films with superior thermal conductivity, Sci. Rep. 5 (2015) 14260.
[39] C. Teng, D. Xie, J. Wang, Z. Yang, G. Ren, Y. Zhu, Ultrahigh conductive graphene paper based on ball-milling exfoliated graphene, Adv. Funct. Mater. 27 (20) (2017) 1700240.
[40] D. Lide, CRC Handbook of Chemistry and Physics, 84th ed., Crc Press, Boca Raton, 2003.
[41] C. Kittel, Introduction to Solid State Physics, sixth ed., Wiley, New York, 1986.